European Journal of Nuclear Medicine and Molecular Imaging (2025) 52:2645–2657
https://doi.org/10.1007/s00259-025-07110-8

ORIGINAL ARTICLE

Whole-body PET imaging of simian immunodeficiency virus using gp120-targeting probes fails to reveal regions of specific uptake in rhesus macaques

Sharat Srinivasula[1] · Insook Kim[2] · Hyukjin Jang[1] · Paula Degrange[3] · Heather Brown[3] · Viviana Dalton[3] · Yunden Badralmaa[4] · Ven Natarajan[4] · Brad Long[3] · Jorge A. Carrasquillo[5] · Michele Di Mascio[6]

Received: 23 September 2024 / Accepted: 22 January 2025 / Published online: 31 January 2025
This is a U.S. Government work and not under copyright protection in the US; foreign copyright protection may apply 2025

Abstract

Purpose Following the initial reports demonstrating the feasibility of immunoPET imaging of simian immunodeficiency virus (SIV) using gp120-targeting monoclonal antibodies in non-human primates, replication efforts of the imaging system in human immunodeficiency virus (HIV)-infected individuals have yielded conflicting results. Herein, we used two anti-gp120 antibodies, 7D3 and ITS103.01LS-F(ab')$_2$, to interrogate the reproducibility of gp120-targeting probes for immunoPET imaging of SIV in rhesus macaques.

Methods The binding affinity estimates of ^{89}Zr radiolabeled 7D3 and ITS103.01LS-F(ab')$_2$ to SIV gp120, and the in-vitro and ex-vivo binding specificities of [^{89}Zr]Zr-7D3 and [^{89}Zr]Zr-ITS103.01LS-F(ab')$_2$ to SIV Env expressing cells, primary cells, and tissue sections from uninfected and SIV-infected macaques were obtained through competition assays. The biodistributions of [^{89}Zr]Zr-7D3 and [^{89}Zr]Zr-ITS103.01LS-F(ab')$_2$ were performed with static PET scans up to 6 days post-injection in 20 rhesus macaques and the standardized uptake values in various tissues were compared between SIV-infected and uninfected controls.

Results Despite the demonstrated nanomolar affinity of [^{89}Zr]Zr-7D3 and [^{89}Zr]Zr-ITS103.01LS-F(ab')$_2$ to SIV gp120, and strong binding specificity to SIV gp120 cell lines, we observed no discernible differences in their binding in primary cells, tissue sections of secondary lymphoid organs, in-vivo probe uptake between SIV-infected and uninfected macaques, or ex-vivo validation necropsies. While the probes remained stable in-vivo, only [^{89}Zr]Zr-ITS103.01LS-F(ab')$_2$ in chronic plasma retained its binding specificity to SIV gp120, with [^{89}Zr]Zr-7D3 experiencing a >97% reduction in binding to gp120 due to competition from endogenous antibodies at the 7D3 binding site.

Conclusion The overall absence of specific uptake suggests inadequate binding potential (ligand affinity x target molarity) for these probes to effectively image SIV or HIV in-vivo, warranting further investigation into the lack of reproducibility observed with earlier non-human primate SIV imaging and conflicting human studies.

Keywords ImmunoPET · Rhesus macaques · Endogenous antibodies · 7D3 · ITS103 · Reproducibility

✉ Michele Di Mascio
mdimascio@niaid.nih.gov

[1] AIDS Imaging Research Section, Clinical Monitoring Research Program Directorate, Frederick National Laboratory for Cancer Research, Frederick, MD, USA

[2] AIDS Imaging Research Section, Applied/Developmental Research Directorate, Frederick National Laboratory for Cancer Research, Frederick, MD, USA

[3] AIDS Imaging Research Section, Laulima Government Solutions, Integrated Research Facility, NIAID, NIH, Frederick, MD, USA

[4] Laboratory of Molecular Cell Biology, Frederick National Laboratory for Cancer Research, Frederick, MD, USA

[5] Molecular Imaging Program, Center for Cancer Research, NCI, NIH, Bethesda, MD, USA

[6] AIDS Imaging Research Section, Division of Clinical Research, NIAID, NIH, Poolesville, MD, USA

Introduction

Global efforts are currently advancing to develop immuno-positron emission tomography (immunoPET) HIV-1 imaging systems that combine the targeting specificity of monoclonal antibody (mAb) and the superior sensitivity and spatial resolution of PET to noninvasively monitor tissue sites of viral replication [1–7]. Besides their potentially crucial prognostic value of managing people living with HIV (PLWH), these endeavors could also greatly assist in developing strategies for HIV cures and vaccines [8].

So far, limited pre-clinical immunoPET studies of the nonhuman primate (NHP) model of HIV-1 pathogenesis reported feasibility in achieving this goal with two different viral envelope (Env) specific mAbs. In a simian immunodeficiency virus (SIV) infected rhesus macaque (RM) model undergoing immunoPET imaging with ^{64}Cu radiolabeled PEG-modified intact murine 7D3 mAb (targeting the CCR5 binding site of gp120 envelope glycoprotein [9]), differences in uptake were reported in various lymphoid tissues and the gastrointestinal tract not only between chronically infected viremic and uninfected but also between antiretroviral therapy (ART) treated aviremic and uninfected adult RMs, thus asserting a remarkably sensitive non-invasive imaging system [1, 2]. In a similar NHP model using ^{64}Cu radiolabeled F(ab')$_2$ fragment of primatized 7D3 mAb, viral reactivation in the gut and select lymphoid tissues of long-term ART-treated, aviremic, SIV-infected RMs was reported immediately following administration of a latency reversal agent (LRA), suggesting a sensitive imaging system capable of detecting gp120 in tissues when viral levels are ~3–4 Log$_{10}$ lower than in chronic viremic animals [3, 4]. In another NHP model of simian/human immunodeficiency virus (SHIV)-infected RMs, ^{68}Ga radiolabeled Fab fragment of PGT145 mAb (targeting the variable loop 2 (V2) apex of gp120 [10, 11]) detected viral reactivation in the gastrointestinal tract and some lymphoid tissues immediately following the interruption of long-term ART in infant RMs [5]. Building on this pre-clinical framework, an investigation into the characterization of HIV-1 reservoirs in-vivo with ^{64}Cu radiolabeled 3BNC117 mAb (targeting the CD4 binding site of gp120 [12]) failed to detect HIV-1 Env expression in ART-treated or untreated chronically infected individuals [6]; however, a year later, another clinical trial with ^{89}Zr radiolabeled VRC01 mAb (targeting the CD4 binding site of gp120 [13]) produced some results of significance in select lymph nodes (LNs), bone marrow, and the gut [7]. Despite similarities in the biodistributions of the radiotracers and the PLWH groups imaged in both trials, the reasons for the divergent outcomes remain unclear, especially given the higher binding affinity observed for the radiolabeled 3BNC117.

As longer half-life radionuclides can extend the biodistribution time, which in turn allows for lower background and better clearance of nonspecific uptake, in this study, we utilized ^{89}Zr radiolabeled intact murine 7D3 and ^{89}Zr radiolabeled F(ab')$_2$ fragment of rhesus ITS103.01LS (targeting the CD4 binding site of gp120 [14]) immunoPET to interrogate the whole-body SIV dissemination in-vivo up to 6 days post-radioligand injection and to visualize the localization of SIV virus and viral envelope expressing cells and tissues in chronic and pre-acute infection of adult RMs.

Materials and methods

Animals

Forty-seven juvenile to adult Indian rhesus macaques (RMs) (*Macaca mulatta*) were used in the study following the National Institute of Allergy and Infectious Diseases (NIAID) Animal Care and Use Committee approved protocol. Of the 47 RMs, 20 RMs (designated RM1-RM20) were used for in-vivo PET/CT imaging with [^{89}Zr]Zr-7D3 or [^{89}Zr]Zr-ITS103.01LS-F(ab')$_2$ as outlined in Tables S1-S2 and a few of these RMs also as a source of plasma, cells, or tissue. The remaining 27 RMs (designated RM21-RM47) served exclusively as sources of plasma, primary cells, or tissue for in-vitro studies (Tables S3-S7).

Antibodies, cell lines, and SIV virus

The SIV Env glycoprotein-specific monoclonal antibody (mAb) clone 7D3 was produced from murine 7D3 hybridoma provided by Dr. Jim Hoxie and purified by Protein A affinity chromatography by the AIDS and Cancer Virus Program/Biological Products Core Lab of the Frederick National Laboratory for Cancer Research. HPLC analysis of the 7D3 lots showed 92–100% pure antibody and the sPAGE analysis under reducing conditions demonstrated that the lots consisted almost exclusively of antibody heavy and light chains. Dr. Mario Roederer at the NIH/NIAID/VRC provided the rhesus ITS103.01LS mAb. Dr. Francois Villinger provided the SIV1C cell line and SIVmac239-nef-stop virus. MT4 cell line contributed by Dr. Douglas Richman (catalog #120) and SIVmac251 virus [15] contributed by Dr. Ronald Desrosiers (catalog #253) were obtained through the NIH HIV Reagent Program, Division of AIDS, NIAID, NIH. Dr. Yoshiaki Nishimura provided the SIVmac239 virus.

The SIV1C cells which constitutively express SIV gp120 on the cell surface and activated 24 h prior with PMA (5ng/mL) and Ionomycin (500ng/mL), or MT4 cells infected with SIVmac251 or SIVmac239-nef-stop at a multiplicity

of infection estimated between 0.001 and 0.03 for 6–15 days with a mean viability of 34% (n = 24 kinetics; 95% confidence interval 26-43%) were used as SIV Env expressing cells. The mean viability of uninfected MT4 cells used as negative controls was 91% (n = 15; 95% confidence interval 85-97%).

^{89}Zr radiolabeling of anti-gp120 mAbs

[^{89}Zr]Zr-Df-7D3 and [^{89}Zr]Zr-Df-ITS103.01LS-F(ab')$_2$ were prepared as previously described but with minor modifications [16]. Detailed methods are provided in the supplementary material.

Binding specificity and binding affinity (1/Kd) assays of radiolabeled anti-gp120 mAbs

The in-vitro binding specificities of [^{89}Zr]Zr-7D3 or [^{89}Zr]Zr-ITS103.01LS-F(ab')$_2$ to SIV Env expressing cells, cryopreserved and fresh peripheral blood mononuclear cells (PBMC), lymph node mononuclear cells (LNMC), and spleen cells of RMs were measured as previously described for anti-CD4 mAbs [17]. For detailed methods, see supplementary material.

A secondary binding specificity assessment was also performed by measuring the interaction between [^{89}Zr]Zr-7D3 or [^{89}Zr]Zr-ITS103.01LS-F(ab')$_2$ and SIV gp120 (mac239) protein (eEnzyme LLC) coated on wells. For detailed methods, see supplementary material.

The binding specificity was expressed as the counts per minute (CPM) ratio of total binding (TB) to non-specific binding (NSB). Specific binding was calculated by subtracting the NSB CPM from the TB CPM. The equilibrium disassociation constant K_d, equal to the free ligand concentration at 50% of maximal binding, was estimated from the secondary binding specificity assay using GraphPad Prism 9.3.1 (La Jolla, CA) by fitting the one-site specific binding curve with a weight of $1/y^2$.

Pre-existing immune response against anti-gp120 mAbs

The presence of any pre-existing immune response against 7D3 or ITS103.01LS was tested with radio-HPLC before administration of the radiolabeled mAb for PET/CT imaging as previously described [18]. Briefly, monkey plasma was incubated with [^{89}Zr]Zr-7D3 or [^{89}Zr]Zr-ITS103.01LS-F(ab')$_2$ (mAb concentration 1.5nM-5nM) for 30 min at 37 °C in a humidified 5% CO_2 incubator, and a 50 µl aliquot of the incubated mixture was run through size-exclusion HPLC.

Endogenous proteins competing for the anti-gp120 mAb binding site and immunogenicity of murine 7D3 or rhesus ITS103.01LS-F(ab')$_2$

The presence of endogenous proteins in the plasma that compete for 7D3 or ITS103.01LS-F(ab')$_2$ binding site and the development of immunogenic response post-exposure against the 7D3 or ITS103.01LS-F(ab')$_2$ mAb were detected with a cell binding assay coupled with radio-HPLC as previously described [18]. For detailed methods, see supplementary material.

Stability and binding ability of radiolabeled anti-gp120 mAbs in in-vivo plasma

For the in-vivo stability test, 50µl of the plasma obtained ~ 13 h and ~ 40 h post [^{89}Zr]Zr-7D3 injection or ~ 9 h post [^{89}Zr]Zr-ITS103.01LS-F(ab')$_2$ injection was run through size-exclusion HPLC. For the in-vivo plasma binding ability test, a binding assay with radioactive plasma obtained at 1 h, 2 h, 4 h, 6 h, or ~ 13 h post [^{89}Zr]Zr-7D3 injection or ~ 9 h post [^{89}Zr]Zr-ITS103.01LS-F(ab')$_2$ injection was performed with SIV gp120 expressing cells or SIV gp120 protein coated on wells as described above in the 'Binding specificity' section. Briefly, 1 million viable SIV gp120 expressing cells were incubated with 50 µl of in-vivo radioactive plasma, with or without excess unlabeled mAb, to assess non-specific binding and total binding, respectively. Separately, SIV gp120 coated wells were incubated with 150 µl of in-vivo radioactive plasma, with or without blocking with excess unlabeled mAb. The binding specificity was expressed as the CPM ratio of TB to NSB.

In-vitro autoradiography

The in-vitro binding specificities of [^{89}Zr]Zr-7D3 or [^{89}Zr]Zr-ITS103.01LS-F(ab')$_2$ to axillary and inguinal lymph nodes, spleen, colon, and jejunum tissues were measured with autoradiography. For detailed methods, see supplementary material.

PET/CT imaging and data analysis

In-vivo PET imaging was performed with MultiScan LFER 150 PET/CT camera (Mediso Medical Imaging Systems, Budapest, Hungary) designed for nonhuman primates. See the supplementary material for the acquisition and post-processing parameters used.

PET images were analyzed using MIM software (Cleveland, USA), independently and blindly by three operators (authors: SS, HJ, and JAC). Volumes of interest (VOI) on the co-registered PET and CT image were manually drawn for

cervical, axillary, and inguinal lymph nodes (LNs), spleen, heart (blood pool), liver, left kidney, bone marrow, muscle, and gut, and the amount of radioligand uptake was quantified as maximum and/or mean standardized uptake value (SUV) using the formula: SUV = (*c/d)*w*, where *c* is decay-corrected tissue concentration (kBq/mL), *d* is the injected dose (kBq), and *w*, the body weight (g). Bone marrow uptake was evaluated at three locations: L4 lumbar vertebrae, entire thoracic and lumbar vertebrae, and the proximal humerus. Muscle uptake was measured by drawing VOI on the back muscles adjacent to the spine at the axial level of the heart. Care was taken to avoid any abdominal LNs in the gut VOI. Images and the quantitative measures were not corrected for the partial volume effect.

Statistical analysis

Unpaired samples were compared with the non-parametric Wilcoxon rank-sum test and the relationship between variables in the cross-sectional analysis was assessed with Spearman rank correlation using Winstat software (Cambridge, MA). A P-value < 0.05 was considered statistically significant.

Results

In-vitro performance of [^{89}Zr]Zr-7D3

Stability of [^{89}Zr]Zr-7D3

From radio-HPLC tests, [^{89}Zr]Zr-7D3 stored in PBS was stable at 4°C for at least 5 days and at 37°C for at least 42 h post-radiolabeling (Fig. S1 a).

Binding affinity and binding specificity of [^{89}Zr]Zr-7D3 to SIV Env expressing cell lines, SIV gp120 coated wells, and primary cells from SIV-infected macaques

[^{89}Zr]Zr-7D3 bound to SIV gp120 protein with a nanomolar affinity (the average equilibrium disassociation constant K_d ~0.35nM from 3 saturation binding assays; Fig. S1 b). Binding assays with [^{89}Zr]Zr-7D3 concentration ranging from 0.15nM to 6.7nM showed an average binding specificity (expressed as total binding to non-specific binding ratio) to SIV Env expressing cells (activated SIV1C, or MT4 cells infected in-vitro with SIVmac251 or SIVmac239-nef-stop) of 7.6 (range 2.6–24.7; $n = 19$ assays; 8 assays at 0.15nM, 8 assays at 0.5nM, and 1 assay each at 1nM, 3nM, and 6.7nM concentration). Similarly, the average binding specificity of [^{89}Zr]Zr-7D3 at concentrations ranging from 0.1nM to 7nM to SIV gp120 protein coated on wells was 4.7 (range 3.0–6.8; 3 assays each at 0.1, 0.5, 1, 3, 5, and 7nM). However, the binding specificities of [^{89}Zr]Zr-7D3 to peripheral blood mononuclear cells (PBMC), lymph node mononuclear cells (LNMC), and spleen cells from chronically SIV-infected RMs (Table S3) at 0.5nM concentration were similar to the binding specificity of ≈1 observed in negative control cells (cells from uninfected RMs or uninfected MT4 cells). These data suggest a lack of specific uptake of the radiolabeled 7D3 to primary infected lymphocytes from SIV-infected RMs.

Autoradiography of [^{89}Zr]Zr-7D3

To further explore evidence of specific uptake in lymphoid organs not explained by gp120 expressed on the surface of infected cells, we performed autoradiography studies on tissue sections obtained from both SIV-infected and uninfected animals. The autoradiography of LN, spleen, and gut tissue sections from chronically SIV-infected RMs paired with uninfected controls and competed with excess unlabeled 7D3 also did not detect differences in bound [^{89}Zr]Zr-7D3 (Table S4).

In-vivo performance of [^{89}Zr]Zr-7D3

PET/CT imaging of chronic SIV-infection

After ensuring with radio-HPLC of no formation of immune complexes due to any pre-existing immune response in RMs against the 7D3 mAb or due to other endogenous proteins that may interfere with the antigen binding site of 7D3, we administered [^{89}Zr]Zr-7D3 intravenously in five chronically SIV-infected RMs and six uninfected controls (Table S1). All 11 RMs underwent PET/CT scanning at ~40 h, and 9 of the 11 RMs were scanned again on Day 5–6 post [^{89}Zr]Zr-7D3 administration. To corroborate in-vivo observations, we euthanized one chronically SIV-infected RM and one uninfected control (RM1 and RM8) soon after their ~40 h scan, and another pair (RM4 and RM13) on Day 7 post [^{89}Zr]Zr-7D3 administration, harvested their organs, removed contents from the bowel, and measured the radioactivity in tissues using a gamma counter. Despite high levels of specificity of binding of [^{89}Zr]Zr-7D3 to gp120 was observed in in-vitro assays, no marked differences of [^{89}Zr]Zr-7D3 uptake in the PET images were evident visually and semi-quantitatively in any organs, including LNs, spleen, and the gut between the uninfected and the chronic SIV-infected RMs (Fig. 1 and Fig. S2). Of note, the radiotracer uptake observed in the colon of the SIV chronically infected RM3, and at a lower intensity in the uninfected control RM10, in the 40 h PET scan disappeared at Day 5 (Fig. 1a), suggesting a non-specific intraluminal probe

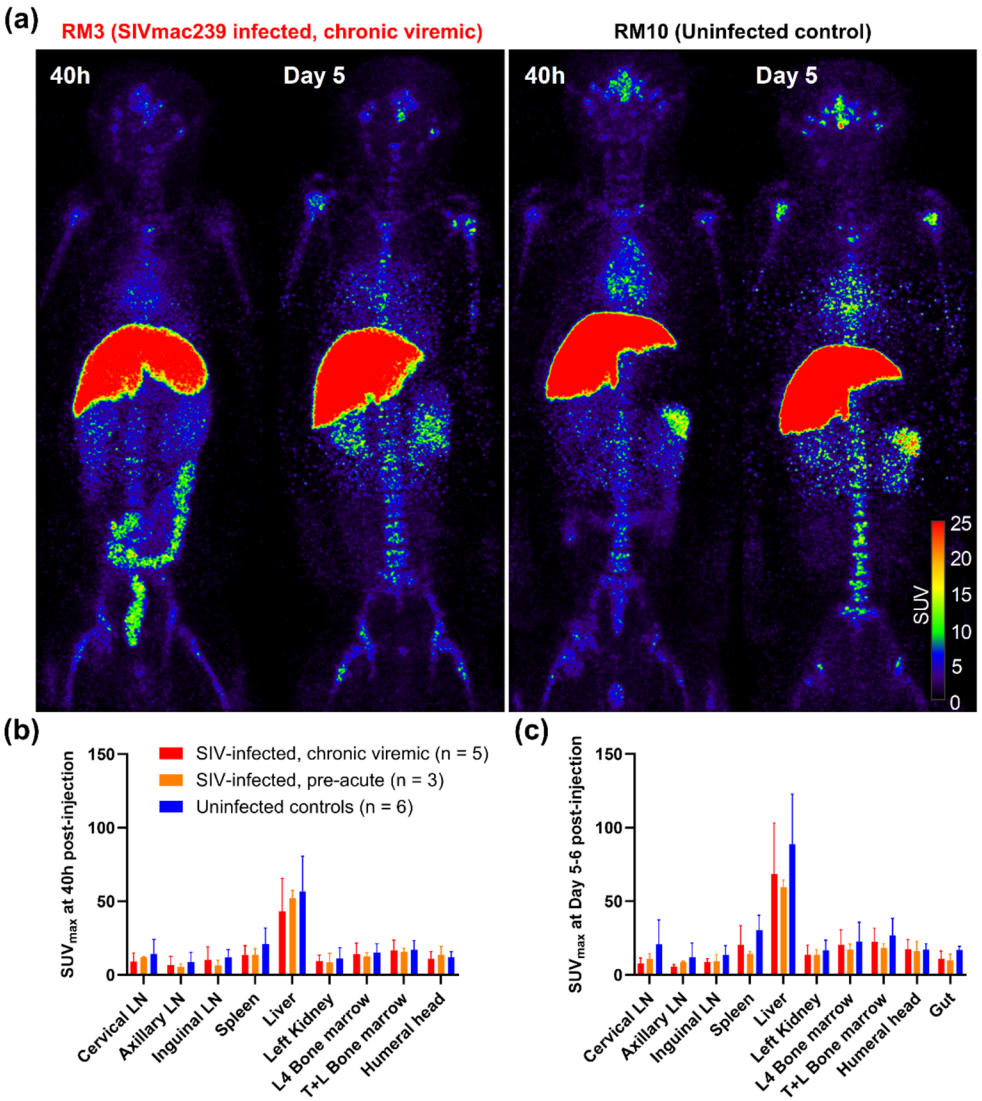

Fig. 1 Maximum intensity projection in-vivo PET images of a representative chronically SIV-infected viremic rhesus macaque (RM3) and a representative uninfected control (RM10) following administration of ~1 mg mass of [^{89}Zr]Zr-7D3 (~30MBq of ^{89}Zr) and scanned at 40 h and Day 5 post-injection **(a)**. Tissue uptakes were converted to RAINBOW color map as shown in the color bar, where red color indicates the high standardized uptake value (SUV). Comparison of maximum SUV (SUV_{max}) in tissues among the chronically SIV-infected viremic (red), pre-acutely SIV-infected (orange), and uninfected controls (blue) at 40 h (**b**) and Day 5–6 (**c**) post-injection. Both visual and semi-quantitative SUV analysis showed no higher uptake in the SIV-infected RMs compared to the uninfected controls. Because of intraluminal uptake in some animals at 40 h, the gut uptake is not plotted. Plots are mean values and error bars are standard deviation

excretion. Similar levels of bowel clearance of the probe were observed in other SIV-infected and uninfected animals. The ex-vivo tissue analysis agreed with the in-vivo observations (Fig. S3a, b).

At any time point measured post-injection, we observed no significant differences in the standardized uptake value (SUV) of [^{89}Zr]Zr-7D3 in the peripheral blood and plasma between SIV-infected and uninfected (P = NS; Fig. S4b, c). Using the radioactive plasma obtained at ~13 h post-injection (mean ± standard deviation estimated [^{89}Zr]Zr-7D3 concentration in the plasma was 7.1 ± 2.9nM (n = 11)), we performed a binding assay in a subgroup of animals (4 chronically infected and 3 uninfected). [^{89}Zr]Zr-7D3 in the plasma retained its binding specificity to SIV gp120 only in the uninfected controls but not in the chronically infected RMs in which > 97% reduction in binding to gp120 was observed. Even in the binding assay with radioactive plasma obtained at earlier times (1 h, 2 h, 4 h, and 6 h post-injection) when [^{89}Zr]Zr-7D3 concentration was much higher (calculated to be ~18nM at 1 h post-injection, n = 3 (2 chronically infected and 1 uninfected)), we observed a near full loss of [^{89}Zr]Zr-7D3 binding to gp120 in the plasma of the chronically infected RMs at all time points, but not in the uninfected plasma (data not shown).

In-vivo Stability of [^{89}Zr]Zr-7D3

Radio-HPLC of the plasma obtained at ~13 h (data not shown) and ~40 h post [^{89}Zr]Zr-7D3 injection in all 11 RMs (5 chronically SIV-infected and 6 uninfected RMs) confirmed near 100% stability of [^{89}Zr]Zr-7D3 in-vivo, and we detected no formation of high molecular weight complexes nor breakdown to small molecules (Fig. S1 d), suggesting that the binding loss of [^{89}Zr]Zr-7D3 probe in the plasma of the chronically SIV-infected RMs was likely due to high

concentrations of endogenous proteins competing for the 7D3 binding site.

Development of endogenous proteins in SIV-infected macaques that compete for the 7D3 binding site

To explore the rapid loss of binding of [^{89}Zr]Zr-7D3 probe in the plasma of the chronically SIV-infected RMs, we tested the in-vitro binding of [^{89}Zr]Zr-7D3 to SIV Env expressing cells in the presence of uninfected or chronic plasma (Table S5). The 7D3 binding in the presence of chronic plasma was fully abrogated, with the binding similar to non-specific binding wells where Env+cells were pre-incubated with ~3–4 Log_{10} higher concentration of the unlabeled 7D3. We then tested the emergence of binding inhibition in five RMs intravenously inoculated with 200 $TCID_{50}$ of SIVmac239-nef-stop and followed longitudinally [19]. Binding assay in the presence of plasma revealed no loss of 7D3 binding to SIV Env expressing cells at Day 7 post-inoculation (p.i.), 0–51% loss at Day 14 p.i., and near full binding abrogation by week 5 p.i (Fig. 2a). Radio-HPLC of the incubated [^{89}Zr]Zr-7D3+plasma mixture revealed no formation of high molecular weight immune complexes and >90% of the radioactivity of the injected [^{89}Zr]Zr-7D3+plasma mixture eluted with a retention time identical to that of [^{89}Zr]Zr-7D3, suggesting that the binding inhibition was due to endogenous proteins, likely antibodies, in the chronic plasma competing for the 7D3 binding site and not due to the blockade of the 7D3 antigen binding site (Fig. S1 e). A similar gradual 7D3 binding loss was also observed during SIVmac251- and SIVmac239-infection where endogenous proteins competing for 7D3 binding site were either absent or below the assay detection levels in the plasma for at least until 10 days post-inoculation (Fig. 2b, c). Though no loss of 7D3 binding to SIV Env expressing cells was observed in the presence of pre-acute plasma, the binding specificity of [^{89}Zr]Zr-7D3 to Day 7 and Day 10 PBMC was ≈1 (Table S3).

After five weeks of SIVmac239-nef-stop infection, the five RMs initiated a 13-week course of daily antiretroviral therapy (ART) [19]. At the end of 13 weeks of effective ART, we observed a reduced loss in 7D3 binding to Env+cells in the presence of ART-suppressed plasma (plasma viral load (PVL)<10 copies/mL) (Fig. 2a, e). Three weeks following ART interruption, a near-complete abrogation of 7D3 binding, and during the chronic phase of infection, a complete 7D3 binding abrogation was observed in all five SIVmac239-nef-stop-infection RMs (Fig. 2a). However, in a group of four SIVmac251 infected macaques that were rectally challenged with 1000 $TCID_{50}$ and chronically infected for over 1 year before initiating ART, complete inhibition of 7D3 binding to Env+cells was observed in the presence of ART-suppressed plasma (on ART for >6 months (range 32 to 78 weeks), PVL<50 copies/mL at least for the last 6 months) (data not shown).

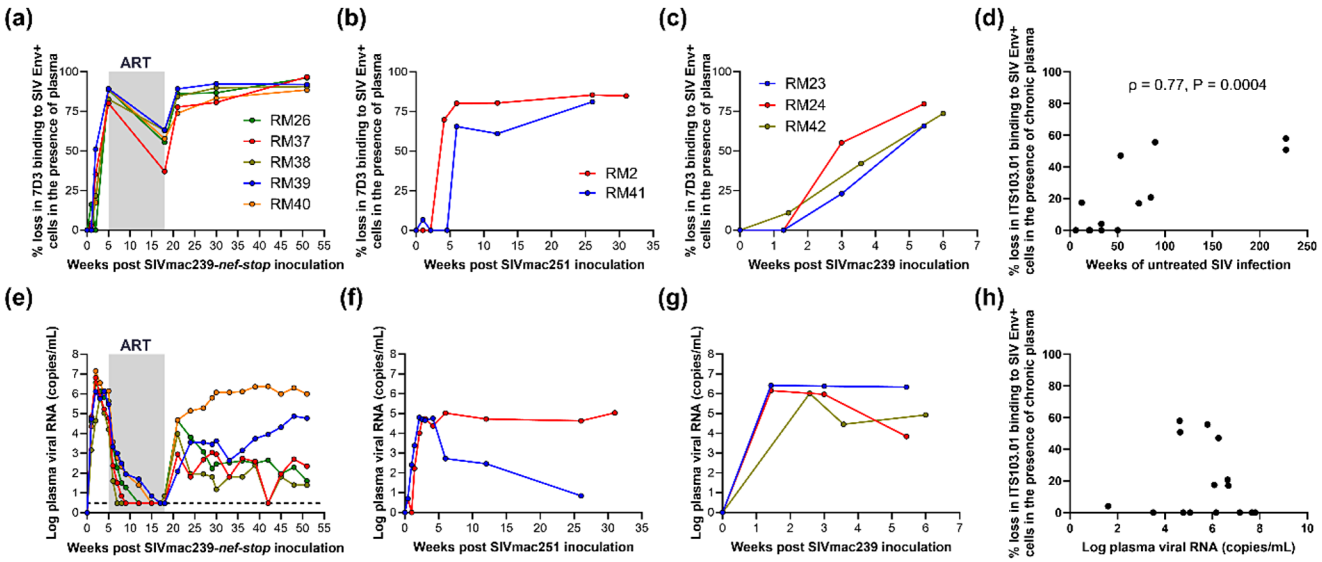

Fig. 2 Percent loss of 7D3 binding to SIV Env+cells in the presence of plasma from 5 rhesus macaques intravenously inoculated with 200 $TCID_{50}$ SIVmac239-nef-stop **(a)**, 2 rhesus macaques intravenously inoculated with 300 $TCID_{50}$ SIVmac251 **(b)**, 3 rhesus macaques intravenously inoculated with 1000 $TCID_{50}$ SIVmac239 **(c)**, and their respective plasma viral RNA (**e**, **f**, **g**). Percent loss of ITS103.01LS-$F(ab')_2$ binding to SIV Env+cells in the presence of chronic plasma from 15 rhesus macaques infected with either SIVmac239 or SIVmac239-nef-stop and either antiretroviral therapy naïve or off antiretroviral therapy (**d**, **h**). The horizontal dashed line in panel E indicates the minimum detection threshold of 3 copies/mL. In panel D, ρ is the Spearman rank correlation coefficient and P is one-sided significance

PET/CT imaging of pre-acute SIV-infection with [^{89}Zr]Zr-7D3

As the failure of [^{89}Zr]Zr-7D3 to highlight in-vivo differences of SIV Env expression between chronically infected and uninfected controls could in part be due to excess levels of endogenous proteins competing for the gp120 binding site of 7D3, we hypothesized that the potential to observe in-vivo SIV Env expression could be during pre-acute infection before an antibody response to gp120 was mounted. So, we intravenously inoculated three RMs with SIVmac239 (Table S1). After screening for any pre-existing immune response against the 7D3 mAb and also confirming the absence of interfering and competing endogenous proteins in the plasma on Day 7 of SIV-infection, we administered [^{89}Zr]Zr-7D3 on Day 8 of SIV-infection and performed PET/CT imaging at ~40 h (Day 10), optionally at ~90 h (Day 12), and ~108–132 h (Day 13–14) post [^{89}Zr]Zr-7D3 administration. Radio-HPLC of the plasma obtained at ~10 h (data not shown) and ~40 h post [^{89}Zr]Zr-7D3 injection confirmed near 100% stability of [^{89}Zr]Zr-7D3 in-vivo (Fig. S1d). Both qualitative and semi-quantitative SUV analyses of various lymphoid tissues and the gut failed to show higher uptake in the SIV-infected compared to the uninfected controls. (Fig. S2, S5, and Fig. 1b and c).

Since the levels of viral RNA in lymphoid tissues were shown to be similar between Day 7–10 post-infection and the chronic phase of SIV-infection [20–22], we combined the five chronic and three pre-acutely infected RMs and compared the uptake with the six uninfected controls. We observed no statistically significant differences in the radiotracer uptake between SIV-infected and uninfected controls (P = NS).

Immunogenicity of [^{89}Zr]Zr-7D3

We tested the immunogenicity of the murine 7D3 mAb probe 5–11 weeks after exposure in 9 of 14 RMs (2 chronic, 3 pre-acute, and 4 uninfected). Though HPLC showed no formation of high molecular weight immune complexes in all 4 uninfected RMs and the 2 chronic RMs after the exposure, 2 of 3 acutely SIV-infected macaques developed an immune response against the 7D3 mAb.

Though comparably viremic, the pre-acute infection may not translate to similar gp120 concentrations present in the tissues of chronically infected animals. To image chronic infection, we found ITS103.01LS to be a promising mAb with good binding affinity and binding specificity to SIV gp120, and also less unaffected by the barrier of competing endogenous proteins consistently detected for 7D3.

In-vitro performance of [^{89}Zr]Zr-ITS103.01LS-F(ab')2

Stability of [^{89}Zr]Zr-ITS103.01LS-F(ab')2

[^{89}Zr]Zr-ITS103.01LS-F(ab')$_2$ stored in PBS was stable at 4°C for at least 6 days and at 37°C for at least 48 h post-radiolabeling as assessed by radio-HPLC (Fig. S1f).

Binding affinity and binding specificity of [^{89}Zr]Zr-ITS103.01LS-F(ab')$_2$to SIV Env expressing cell lines, SIV gp120 coated wells, and primary cells from SIV-infected macaques

Saturation binding assays of [^{89}Zr]Zr-ITS103.01LS-F(ab')$_2$ showed a nanomolar affinity to gp120 (K_d ~0.87nM, n = 4 assays; Fig. S1c). In binding assays at 0.5nM concentration of [^{89}Zr]Zr-ITS103.01LS-F(ab')$_2$, we observed an average binding specificity of 6.1 (range 3.2–8.7; n = 9 assays) to SIV Env expressing cells (MT4 cells infected in-vitro with SIVmac239-nef-stop) and an average binding specificity of 5.4 (range 4.8–6.0; n = 5 assays) to SIV gp120 coated on wells. Yet, as observed with 7D3, the binding specificities of [^{89}Zr]Zr-ITS103.01LS-F(ab')$_2$ to PBMC, LNMC, and spleen cells of chronically SIV-infected RMs (Table S6) at 0.5nM concentration were similar to the binding specificity to cells from uninfected controls or uninfected MT4 cells of ≈1.

Autoradiography of [^{89}Zr]Zr-ITS103.01LS-F(ab')2

No differences in the binding specificity of [^{89}Zr]Zr-ITS103.01LS-F(ab')$_2$ were noted on the autoradiography of LN, spleen, and gut tissue sections from chronically SIV-infected RMs compared with uninfected controls or when competed with excess unlabeled ITS103.01LS (Table S7).

Endogenous proteins in SIV-infected macaques competing for the ITS103.01LS-F(ab')2 binding site

Though we still observed some loss of ITS103.01LS-F(ab')$_2$ binding to SIV Env expressing cells in the presence of some chronic plasma samples due to competing endogenous proteins, the loss was more variable and significantly lower than 7D3 binding loss (% loss = 0–58%, average loss = 18%, n = 15, Log_{10} PVL range = 1.6–7.8 copies/mL) with some animals showing no loss, and as expected, the loss strongly correlated with the length of untreated SIV-infection (ρ = 0.77, P < 0.001, Fig. 2d).

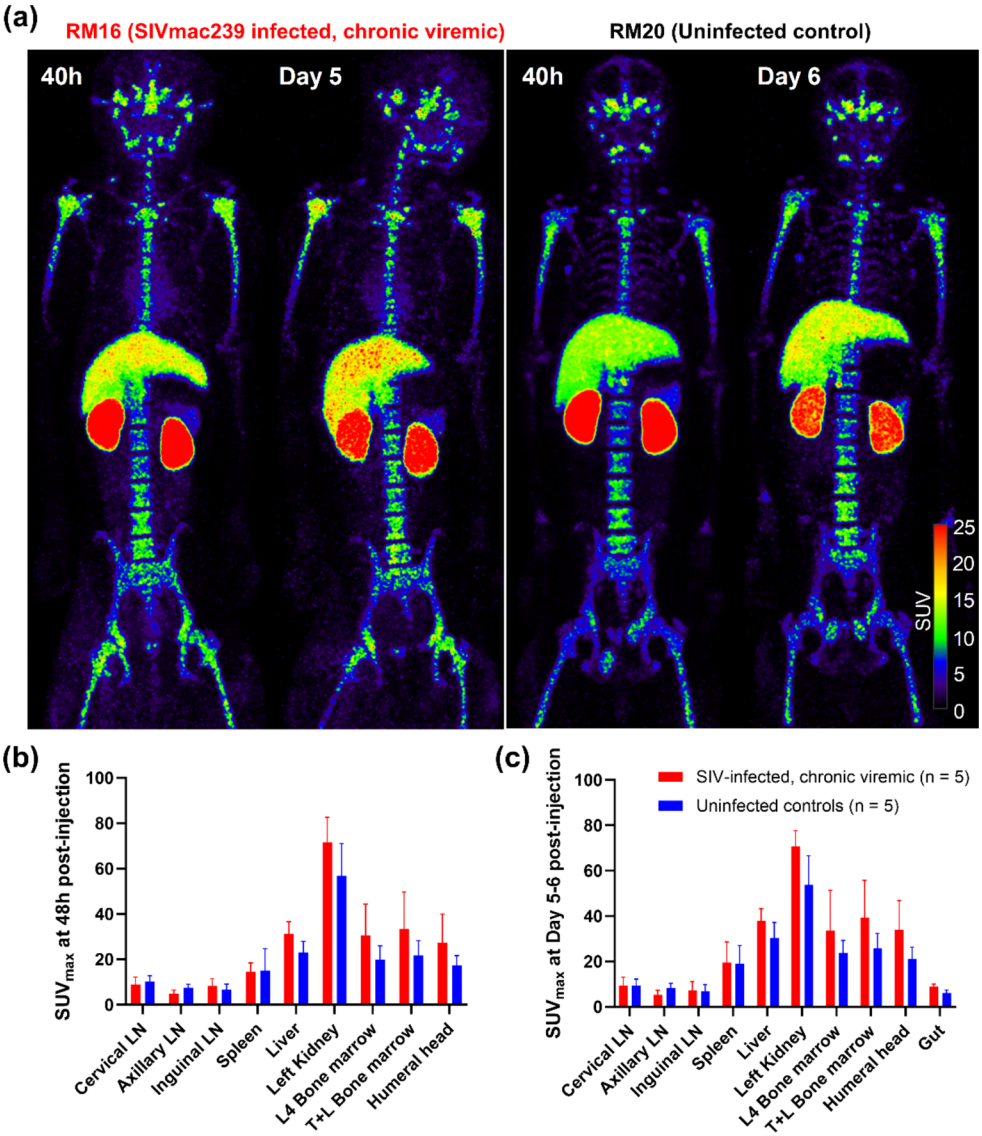

Fig. 3 Maximum intensity projection in-vivo PET images of a representative chronically SIV-infected viremic rhesus macaque (RM16) and a representative uninfected control (RM20) following administration of ~1 mg mass of [^{89}Zr]Zr-ITS103.01LS-F(ab')$_2$ (~74MBq of ^{89}Zr) and scanned at 48 h and Day 5–6 post-injection **(a)**. Tissue uptakes were converted to RAINBOW color map as shown in the color bar, where red color indicates the high standardized uptake value (SUV). Comparison of maximum SUV (SUV_{max}) in tissues among the chronically SIV-infected viremic (red) and uninfected controls (blue) at 48 h (**b**) and Day 5–6 (**c**) post-injection. Both visual and semi-quantitative SUV analysis showed no higher uptake in the SIV-infected RMs compared to the uninfected controls. Because of intraluminal uptake in some animals at 48 h, the gut uptake is not plotted. Plots are mean values and error bars are standard deviation

In-vivo performance of [^{89}Zr]Zr-ITS103.01LS-F(ab')2

PET/CT imaging of chronic SIV-infection We administered [^{89}Zr]Zr-ITS103.01LS-F(ab')$_2$ in five SIVmac239 chronically infected RMs and five uninfected controls (Table S2) and performed PET/CT scans at ~48 h and Day 5–6 post-injection. In two RMs (RM10 and RM16) we observed the formation of high molecular weight complexes without loss in binding to SIV Env expressing cells, and in two other RMs (RM3 and RM15) we detected endogenous proteins competing for the binding site of ITS103.01 mAb resulting in ~20% loss of binding of [^{89}Zr]Zr-ITS103.01LS-F(ab')$_2$ to SIV Env expressing cells. The plasmas of all other animals showed no changes in the molecular weight of the probe and no loss of binding of the probe to SIV Env expressing cells. Both qualitative and semi-quantitative PET SUV analysis of various lymphoid tissues and the gut failed to show higher uptake in the chronic SIV-infected RMs compared to the uninfected controls (Fig. 3 and Fig. S6). The probe uptake observed in the gut of some RMs at 48 h cleared by Day 5 and is consistent with intraluminal uptake (data not shown). Two RMs (RM3 and RM17) were euthanized soon after their Day 5 imaging and organs were harvested to corroborate in-vivo observations. The ex-vivo tissue analysis in a gamma counter agreed with the in-vivo images (Fig. S3c).

In-vivo stability of [^{89}Zr]Zr-ITS103.01LS-F(ab')2

We obtained plasma at ~9 h post [^{89}Zr]Zr-ITS103.01LS-F(ab')$_2$ injection in 8 of the 10 RMs (4 chronically infected and 4 uninfected). Radio-HPLC of that plasma confirmed near 100% stability of the radiotracer in-vivo (Fig. S1g), and a binding assay confirmed the probe in the plasma of

all 8 RMs (mean (±standard deviation) estimated [^{89}Zr]Zr-ITS103.01LS-F(ab')$_2$ concentration was 10.0 (±1.5)nM (n=8)) retained its binding specificity to SIV Env expressing cells. As the [^{89}Zr]Zr-ITS103.01LS-F(ab')$_2$ tracer cleared faster than [^{89}Zr]Zr-7D3 (Fig. S4e, f), we could not run in-vivo stability analysis with HPLC at later time points. However, [^{89}Zr]Zr-ITS103.01LS-F(ab')$_2$ incubated with RM plasma in-vitro at 37ºC was near 100% stable for at least 48 h.

Immunogenicity of [^{89}Zr]Zr-ITS103.01LS-F(ab')2

We tested the immunogenicity of the rhesus [^{89}Zr]Zr-ITS103.01LS-F(ab')$_2$ mAb probe 5–10 weeks after exposure in 5 of 10 RMs (3 chronic and 2 uninfected). Radio-HPLC assay showed no development of immune response against the ITS103.01LS-F(ab')$_2$ mAb in all 5 RMs tested, nor were there changes in immunoreactivity.

Discussion

Two pre-clinical studies by Santangelo et al. [1, 2] using 7D3 mAb, targeting gp120, claimed feasibility to non-invasively detect, localize, and quantify viral sites in chronic and acute SIV infection, as well as the residual virus in antiretroviral-treated aviremic RMs (when the viral RNA in lymphoid tissues is reduced by ~4 Log_{10}). Therefore, we selected the same 7D3 mAb, radiolabeled it with ^{89}Zr, and observed an in-vitro binding specificity of ~8 to SIV cell lines. However, the binding specificity to primary cells (PBMC, LNMC, and spleen cells; freshly isolated and/or cryopreserved) from SIV-infected RMs was ~1, indicating a lack of specific binding. In contrast, with [^{64}Cu]Cu-DOTA-7D3-PEG, Santangelo et al. [1] reported an in-vitro binding specificity of ~3 using cell lines, and ~2–3 to the spleen and LN cells from SIV-infected RMs. Of note, Santangelo et al. used cryopreserved (but not freshly isolated) cells from fewer animals and without an unlabeled mAb competition assay, all potential factors contributing to the discrepancy with their study.

Since not all gp120 in tissue is expressed on the primary cells, we also performed autoradiography, an ex-vivo validating technique that often yields data with robust predictive power regarding the feasibility of imaging a target in-vivo, which was lacking in all previous studies claiming the feasibility of imaging SIV\SHIV\HIV viral replication in-vivo. Autoradiographic analyses of [^{89}Zr]Zr-7D3 consistently showed no differences between total binding and non-specific binding of tissue sections from several lymphoid organs of SIV-infected animals or compared to uninfected animals.

Consistent with the ex-vivo measurements, we found no discernible differences in [^{89}Zr]Zr-7D3 uptake in any organs between SIV-infected and uninfected animals in-vivo. Radio-HPLC analyses of the radiotracer circulating in the plasmas of imaged animals confirmed high stability of [^{89}Zr]Zr-7D3 in-vivo. We detected evidence of endogenous interference (likely antibodies) competing for the binding site of 7D3 in SIV chronically infected RMs at concentrations sufficient to fully abrogate binding of the [^{89}Zr]Zr-7D3 to Env+cell lines, i.e., cells with gp120 expressed at levels much higher than primary cells. Santangelo et al. [1] also observed interference of 7D3 binding to Env+cells in the presence of post-infection serum; however, comparing the relative titers of endogenous antibodies between the two studies is not feasible due to the utilization of different assays (flow cytometry [1] vs. radiotracer binding assay in our study). Thus, to explain the discrepant outcomes, one might speculate that our chronic SIV RMs had developed endogenous antibodies at levels higher than those elicited in the animals imaged in all the earlier 7D3 imaging studies [1–4]. This discrepancy could potentially be attributed to unknown colony-specific factors influencing antibody production in response to the same antigen.

The pre-acutely infected animals imaged in our study with [^{89}Zr]Zr-7D3 (with PVL>10^6 SIV-RNA copies/ml), on the other hand, dismiss competing antibodies as a potential explanation for our inability to image the virus in-vivo, because these hosts had not yet had sufficient time, at the time of imaging, to develop such endogenous interference as confirmed through in-vitro plasma binding assays. Although we had not collected tissues at the time of imaging to confirm that sufficiently high levels of viral dissemination in lymphoid organs had been reached, LNs biopsied at week one post-SIVmac infection of both cynomolgus and rhesus macaques have been reported to achieve the cell-associated viral load (CAVL) levels similar to those found in SIV chronically infected animals [20–22]. Nevertheless, it is important to recognize that the gp120 molarity in tissues of SIV- or HIV-infected hosts as well as its association with CAVL-RNA\DNA levels in the same tissues have been minimally investigated to date [23]. To account for all these potentially confounding variables, we next evaluated the performance of a second anti-gp120 radiotracer, [^{89}Zr]Zr-ITS103.01LS-F(ab')$_2$, after discovering evidence of significantly lower (or absent) endogenous antibodies in the plasmas of SIV chronically infected animals competing for its binding to gp120, possibly due to differential immunogenicity of the CCR5 and CD4 binding sites of the gp120. [^{89}Zr]Zr-ITS103.01LS-F(ab')$_2$ also showed high specificity to Env+cells (~6) as well as binding affinity (~1nM) to gp120 similar to those observed for [^{89}Zr]Zr-7D3. Yet, like [^{89}Zr]Zr-7D3, [^{89}Zr]Zr-ITS103.01LS-F(ab')$_2$ also failed to

detect evidence of specific binding to primary cells, autoradiography tissue sections, as well as in-vivo in SIV-chronically infected RMs, including in animals with absent levels of endogenous antibodies competing for the same binding site. Both [^{89}Zr]Zr-7D3 and [^{89}Zr]Zr-ITS103.01LS-F(ab')$_2$ datasets collectively rule out the possibility that the lack of evidence for specific binding in our study is attributable to higher levels of endogenous antibodies in our infected animals interfering with the binding of the probe to gp120, suggesting that the binding potential (BP; the product of the ligand's affinity and the target's molarity [24]) of these probes is too low for imaging gp120 levels in tissues in-vivo. Indeed, the only evidence of specific binding in our study was observed in gp120-expressing cell lines. Of note, CAVL measured in SIVmac-infected MT4 cell lines with binding specificity of 5.1–7.9 was ~10^{10}-10^{11} copies/million cells (data not shown), hence ~5 Log_{10} higher than the typical SIV-RNA levels observed in the LNs or rectal tissues of highly viremic chronically SIV-infected RMs [19], and ~8–9 Log_{10} higher than the residual viral replication in ART-treated, PVL-suppressed, SIV-infected RMs [19].

Despite utilizing similar mAb mass, injected radioactivity amount, and animal weights, the SUV levels in the two intact 7D3 studies we sought to replicate appear to be dramatically low (up to ~1 Log_{10} lower compared to our study) [1, 2]. While PEGylation could, in principle, affect biodistribution by increasing molecular size, as well as by decreasing non-specific uptake [25], this modification, in our opinion, would not be able to explain the lack of differences in SUV levels between uninfected and infected tissues observed in all our assays (in-vitro, ex-vivo, and in-vivo), nor the lower SUV levels found in their studies. Although the stability, radiochemical purity, and whole-body retention of the radiotracer were not reported in the previous pre-clinical studies, in our study, [^{89}Zr]Zr-7D3 was stable in-vivo and in-vitro, with high whole-body retention (average ~72%) at ~40 h post-injection (Fig. S4a), consistent with the biodistributions of other radiolabeled intact antibodies [26, 27]. Furthermore, the radiometal (^{89}Zr vs. ^{64}Cu) does not appear to account for the observed differences in SUV levels in large organs (e.g. kidneys and liver) between our study and the previous intact 7D3 studies [1, 2] as the biodistribution of the intact 7D3 mAb radiolabeled with ^{64}Cu (^{64}Cu-DOTA-7D3) and PET imaged at 36 h post-injection in our program showed whole-body retention and SUVs in organs similar to those observed with [^{89}Zr]Zr-7D3 (data not shown).

Perplexingly, Santangelo et al. [1] demonstrated evidence of higher SUV levels in the SIV-infected RMs compared to the uninfected RMs not only in LNs and the spleen, the tissues known to harbor high levels of viral dissemination, but also in other organs such as the kidneys, liver, and heart, which typically contain much lower RNA levels [28]. The >2-fold higher uptake of the probe in the heart (blood pool) of infected RMs, indicative of the input function, suggests indeed a non-specific nature of the increase in SUV levels found in other organs, e.g. axillary LNs for which less than 2-fold increase in SUV levels were reported, suggesting a decrease in relative uptake compared to the blood (SUV_{LN}/SUV_{heart}).

Adopting the same NHP immunoPET methodology, in late 2022, Samer et al. [3] claimed the feasibility of imaging LRA-induced viral reactivation in tissues of long-term antiretroviral-treated aviremic SIV-infected RMs using the non-pegylated F(ab')$_2$ fragment of the primatized 7D3 radiolabeled with ^{64}Cu, although no in-vitro binding data in primary cells or tissue sections were provided to corroborate their observations, nor included an uninfected control arm. Increased SUV levels were reported in axillary LNs and the gut following one cycle of the LRA administration for one or two weeks but without concomitant increases in heart SUV levels. However, we believe that those asymmetrical SUV increases observed in axillary LNs ipsilateral to the injection site combined with the lack of increase in uptake in other clusters of LNs (e.g. the inguinal LNs which showed increases in viral RNA levels following the LRA administration comparable to axillary LNs) likely indicate fully non-specific uptake due to accidental infiltration of the probe into subcutaneous space observed in the imaging time points post-LRA administration but not in the baseline imaging time points of several RMs (four out of the five animals for which increase in nodal SUV levels were reported). Subcutaneous administration of radiolabeled antibodies is known to result in non-specific LN uptake [29]. The gut uptake, moreover, appears consistent with intraluminal excretion, also observed with other radiolabeled intact mAbs or mAb fragments [7, 30], which seems included in their studies given how their regions of interest were drawn. Of note, similar high levels of probe uptake in the gut were observed in some animals in our study at 40–48 h post-injection, which dramatically cleared by Day 5 post-injection (a phenomenon that we were able to observe in our study due to the longer half-life of the ^{89}Zr compared to ^{64}Cu), again indicating a non-specific nature of such uptake.

More recently (Kim et al. [4]), the same team conducted the same immunoPET imaging during multiple cycles of 2-week on/2-week off LRA administration at higher doses while the RMs were on suppressive ART. A notable rise in LN and gut SUV levels during the third cycle coincided with increased blood pool (heart) and liver SUV uptake. In conjunction with the earlier NHP studies by Santangelo et al. where increased LN uptake coincided with increased heart activity, it suggests the latter is necessary for observing increased LN SUV levels with their imaging system.

This holds especially true if we consider the LN increase reported in Samer et al. occurring without a corresponding heart increase was due to tracer extravasation. Further discussion of Kim et al. [4] is provided in the supplementary material.

In summary, given that the increase in SUV levels in tissues has been observed in these four NHP immunoPET studies [1–4] only when there is a concomitant increase in SUV levels of the heart, that none of these studies have documented evidence of specific uptake ex-vivo in tissues, and that the evidence of specific uptake in primary cells was reported only in the first publication with a limited number of samples and without competition assay [1], we believe that the feasibility of imaging SIV in-vivo with immunoPET using gp120-targeting antibodies\fragments with nanomolar affinities has not been demonstrated to date and the discrepancy in the biodistribution between our study and earlier NHP imaging studies remains unexplained. Therefore, it is crucial, given the state-of-the-art research in this novel area of imaging science, to contextualize the efforts of the past decade in demonstrating the feasibility of imaging SIV/HIV viral replication *in-viv*o using non-invasive nuclear medicine technologies and compare with milestones achieved in other areas of imaging viruses in-vivo.

Two decades ago, when imaging science initiatives began harnessing nuclear medicine technologies for in-vivo viral replication imaging [31], the consensus in the field was that only the herpes simplex virus (HSV) could be imaged in-vivo with a radiolabeled tracer. This was achieved by exploiting a mechanism of signal amplification through viral thymidine kinase (TK), which phosphorylates and traps the probe within infected cells. Imaging viruses that lack such enzymes for signal amplification was anticipated to rely primarily on quantitative aspects of ligand-receptor mechanisms, such as radiolabeling antibodies to specific targets on virions or infected cells. In general, the feasibility of imaging a target with this mechanism primarily depends on BP, which must be sufficiently high for successful in-vivo imaging of the virus. Additionally, for a given BP, the higher the association rate, the greater the feasibility of imaging the target at earlier timepoints post-injection. However, other factors beyond BP, such as biodistribution, may prevent the imaging system from visualizing the viral target in-vivo, emphasizing the importance of ex-vivo autoradiography studies to predict success in imaging viruses in-vivo [31]. To clarify, the presence of specific uptake in tissue sections from infected hosts suggests the potential for detecting the virus in vivo. Conversely, the absence of such evidence in autoradiography tissue sections indicates a considerable setback in the feasibility of in-vivo viral imaging.

The lack of specific uptake observed in our study in primary cells and tissues obtained from SIV-infected hosts with two different probes exhibiting nanomolar binding affinities to two different sites of the gp120 suggests that the BP of such probes may not be sufficiently high to succeed in imaging SIV in-vivo. If our negative findings are validated, alternative imaging approaches should be interrogated involving higher affinity ligands for gp120, although to our knowledge no such ligands are yet reported in the literature, or other viral targets such as internal viral proteins like capsid, which are the most abundant, or proteases, especially considering their reported picomolar affinity [31]. Additionally, examining mechanisms of signal amplification, as proposed by Bhaumik et al. [32] warrants investigation in preclinical settings.

Yet, inspired by the successes claimed in the earlier SIV NHP publications, two clinical imaging studies utilizing non-pegylated gp120-targeting bNAbs, [^{89}Zr]Zr-VRC01 (Beckford-Vera et al. [7]) and [^{64}Cu]Cu-3BNC117 (McMahon et al. [6]), undertook to non-invasively image HIV-1 but reached conflicting conclusions – while McMahon et al. [6] did not detect Env expression in HIV-chronically infected viremic individuals, Beckford-Vera et al. [7] observed higher mAb uptake in some lymphoid tissues compared to uninfected controls. However, it is important to acknowledge that the absolute increase in SUV levels observed in the LNs and gut in the [^{89}Zr]Zr-VRC01 study is only ~ 10–20% of the SUV levels in the heart (blood pool), hence close to background levels as can be clearly appreciated by their maximum intensity projection images, and no significant differences in spleen uptake was observed. Additional discussion of the two clinical trials is provided in the supplementary material.

Inspired by the first SIV NHP imaging study [1], immunoPET methodologies are being adapted to image SARS-CoV-2 infected NHPs [33]. We anticipate that the outcomes of these investigations will be influenced by quantitative considerations regarding the relative BP of the proposed radiolabeled probes. This involves assessing probe binding affinities and target densities of SIV-gp120, HIV-gp120, and SARS-CoV-2 spike protein in the imaged tissues. For example, the affinities of the anti-HIV-gp120 bNAbs [^{89}Zr]Zr-VRC01 and [^{64}Cu]Cu-3BNC117 mentioned earlier are ~6–15 fold lower and ~2–6 fold lower compared to the affinities of [^{89}Zr]Zr-7D3 and [^{89}Zr]Zr-ITS103.01LS-F(ab')$_2$, respectively. This suggests that assuming similar concentrations of gp120 in SIV and HIV-1 chronically infected hosts with high plasma viremia, the NHP model would likely provide a more sensitive imaging system than imaging the HIV. Conversely, a lack of reproducibility in imaging SIV in-vivo has direct theoretical implications for the feasibility of imaging HIV in-vivo.

In conclusion, further investigation and consideration of various factors are essential to fully comprehend the

implications of the findings from both the preclinical and clinical imaging studies of lentiviral replication discussed above and challenged by our observations. Our study indicates that gp120-targeting antibodies or fragments with nanomolar affinities are insufficient to generate in-vivo images capable of accurately reflecting gp120 concentrations in tissues.

Supplementary Information The online version contains supplementary material available at https://doi.org/10.1007/s00259-025-07110-8.

Acknowledgements We thank the animal care staff and technicians at the NIH Animal Center (Dickerson, Maryland, USA) for their care and handling of the animals, Dr. Jeffrey Lifson, Julian Bess, and Anitha Vijayagopalan for providing the 7D3 mAb, Dr. Mario Roederer for providing the ITS103.01LS mAb, Dr. Ken Matsui, Dr. Hiromi Imamichi and Mindy Smith for technical assistance, and Dr. Marisa St. Claire for veterinary support and technical assistance throughout the study. We thank Dr. Cliff Lane for his ongoing support and useful discussions on the study. We thank Dr. Paolo Lusso for the initial discussions on the study design.

Author contributions S.S., I.K., J.A.C., and M.D.M. conceived the study and designed the research. S.S. and M.D.M. wrote the manuscript with assistance from I.K. and J.A.C.; S.S., H.J., and M.D.M. made the figures and tables. S.S. performed statistical analyses. S.S., I.K., H.J., P.D., H.B., V.D., Y.B., V.N., and B.L. performed research. M.D.M. provided oversight of the study. All authors analyzed and interpreted the data, and critically reviewed the manuscript.

Funding Open access funding provided by the National Institutes of Health
This project has been funded in part with federal funds from the National Cancer Institute, National Institutes of Health, under Contract No. 75N91019D00024. The content of this publication does not necessarily reflect the views or policies of the Department of Health and Human Services, nor does mention of any trade names, commercial products, or organizations imply endorsement by the U.S. Government.

Data availability Data will be made available upon reasonable request.

Declarations

Ethics approval The National Institute of Allergy and Infectious Diseases (NIAID) Animal Care and Use Committee (ACUC) approved all experimental animal protocols.

Competing interests The authors declare no competing financial interests.

Open Access This article is licensed under a Creative Commons Attribution 4.0 International License, which permits use, sharing, adaptation, distribution and reproduction in any medium or format, as long as you give appropriate credit to the original author(s) and the source, provide a link to the Creative Commons licence, and indicate if changes were made. The images or other third party material in this article are included in the article's Creative Commons licence, unless indicated otherwise in a credit line to the material. If material is not included in the article's Creative Commons licence and your intended use is not permitted by statutory regulation or exceeds the permitted use, you will need to obtain permission directly from the copyright holder. To view a copy of this licence, visit http://creativecommons.org/licenses/by/4.0/.

References

1. Santangelo PJ, Rogers KA, Zurla C, Blanchard EL, Gumber S, Strait K, et al. Whole-body immunoPET reveals active SIV dynamics in viremic and antiretroviral therapy-treated macaques. Nat Methods. 2015;12:427–32. https://doi.org/10.1038/nmeth.3320.
2. Santangelo PJ, Cicala C, Byrareddy SN, Ortiz KT, Little D, Lindsay KE, et al. Early treatment of SIV+macaques with an alpha(4) beta(7) mAb alters virus distribution and preserves CD4(+) T cells in later stages of infection. Mucosal Immunol. 2018;11:932–46. https://doi.org/10.1038/mi.2017.112.
3. Samer S, Thomas Y, Arainga M, Carter C, Shirreff LM, Arif MS, et al. Blockade of TGF-beta signaling reactivates HIV-1/SIV reservoirs and immune responses in vivo. JCI Insight. 2022;7. https://doi.org/10.1172/jci.insight.162290.
4. Kim J, Bose D, Arainga M, Haque MR, Fennessey CM, Caddell RA, et al. TGF-beta blockade drives a transitional effector phenotype in T cells reversing SIV latency and decreasing SIV reservoirs in vivo. Nat Commun. 2024;15:1348. https://doi.org/10.1038/s41467-024-45555-x.
5. Obregon-Perko V, Bricker KM, Mensah G, Uddin F, Rotolo L, Vanover D, et al. Dynamics and origin of rebound viremia in SHIV-infected infant macaques following interruption of long-term ART. JCI Insight. 2021;6. https://doi.org/10.1172/jci.insight.152526.
6. McMahon JH, Zerbato JM, Lau JSY, Lange JL, Roche M, Tumpach C, et al. A clinical trial of non-invasive imaging with an anti-HIV antibody labelled with copper-64 in people living with HIV and uninfected controls. EBioMedicine. 2021;65:103252. https://doi.org/10.1016/j.ebiom.2021.103252.
7. Beckford-Vera DR, Flavell RR, Seo Y, Martinez-Ortiz E, Aslam M, Thanh C, et al. First-in-human immunoPET imaging of HIV-1 infection using (89)Zr-labeled VRC01 broadly neutralizing antibody. Nat Commun. 2022;13:1219. https://doi.org/10.1038/s41467-022-28727-5.
8. Deeks SG, Autran B, Berkhout B, Benkirane M, Cairns S, Chomont N, et al. Towards an HIV cure: a global scientific strategy. Nat Rev Immunol. 2012;12:607–14. https://doi.org/10.1038/nri3262.
9. Edinger AL, Ahuja M, Sung T, Baxter KC, Haggarty B, Doms RW, Hoxie JA. Characterization and epitope mapping of neutralizing monoclonal antibodies produced by immunization with oligomeric simian immunodeficiency virus envelope protein. J Virol. 2000;74:7922–35. https://doi.org/10.1128/jvi.74.17.7922-7935.2000.
10. Andrabi R, Voss JE, Liang CH, Briney B, McCoy LE, Wu CY, et al. Identification of common features in Prototype broadly neutralizing antibodies to HIV Envelope V2 apex to facilitate Vaccine Design. Immunity. 2015;43:959–73. https://doi.org/10.1016/j.immuni.2015.10.014.
11. Lee JH, Andrabi R, Su CY, Yasmeen A, Julien JP, Kong L, et al. A broadly neutralizing antibody targets the dynamic HIV Envelope Trimer Apex via a Long, Rigidified, and Anionic beta-hairpin structure. Immunity. 2017;46:690–702. https://doi.org/10.1016/j.immuni.2017.03.017.
12. Scheid JF, Mouquet H, Ueberheide B, Diskin R, Klein F, Oliveira TY, et al. Sequence and structural convergence of broad and potent HIV antibodies that mimic CD4 binding. Science. 2011;333:1633–7. https://doi.org/10.1126/science.1207227.

13. Zhou T, Georgiev I, Wu X, Yang ZY, Dai K, Finzi A, et al. Structural basis for broad and potent neutralization of HIV-1 by antibody VRC01. Science. 2010;329:811–7. https://doi.org/10.1126/science.1192819.
14. Iwamoto N, Mason R, Hu J, Ransier A, Welles H, Song K, et al. A high throughput lentivirus sieving assay identifies neutralization resistant envelope sequences and predicts in vivo sieving. J Immunol Methods. 2019;464:64–73. https://doi.org/10.1016/j.jim.2018.10.013.
15. Daniel MD, Letvin NL, King NW, Kannagi M, Sehgal PK, Hunt RD, et al. Isolation of T-cell tropic HTLV-III-like retrovirus from macaques. Science. 1985;228:1201–4. https://doi.org/10.1126/science.3159089.
16. Vosjan MJ, Perk LR, Visser GW, Budde M, Jurek P, Kiefer GE, van Dongen GA. Conjugation and radiolabeling of monoclonal antibodies with zirconium-89 for PET imaging using the bifunctional chelate p-isothiocyanatobenzyl-desferrioxamine. Nat Protoc. 2010;5:739–43. https://doi.org/10.1038/nprot.2010.13.
17. Di Mascio M, Srinivasula S, Kim I, Duralde G, St Claire A, DeGrange P, et al. Total body CD4+T cell dynamics in treated and untreated SIV infection revealed by in vivo imaging. JCI Insight. 2018;3. https://doi.org/10.1172/jci.insight.97880.
18. Srinivasula S, Gabriel E, Kim I, DeGrange P, St Claire A, Mallow C, et al. CD4+levels control the odds of induction of humoral immune responses to tracer doses of therapeutic antibodies. PLoS ONE. 2017;12:e0187912. https://doi.org/10.1371/journal.pone.0187912.
19. Di Mascio M, Lifson JD, Srinivasula S, Kim I, DeGrange P, Keele BF, et al. Evaluation of an antibody to alpha(4)beta(7) in the control of SIVmac239-nef-stop infection. Science. 2019;365:1025–9. https://doi.org/10.1126/science.aav6695.
20. Huot N, Jacquelin B, Garcia-Tellez T, Rascle P, Ploquin MJ, Madec Y, et al. Natural killer cells migrate into and control simian immunodeficiency virus replication in lymph node follicles in African green monkeys. Nat Med. 2017;23:1277–86. https://doi.org/10.1038/nm.4421.
21. Ziani W, Shao J, Fang A, Connolly PJ, Wang X, Veazey RS, Xu H. Mucosal integrin alpha4beta7 blockade fails to reduce the seeding and size of viral reservoirs in SIV-infected rhesus macaques. FASEB J. 2021;35:e21282. https://doi.org/10.1096/fj.202002235R.
22. Mannioui A, Bourry O, Sellier P, Delache B, Brochard P, Andrieu T, et al. Dynamics of viral replication in blood and lymphoid tissues during SIVmac251 infection of macaques. Retrovirology. 2009;6:106. https://doi.org/10.1186/1742-4690-6-106.
23. Santosuosso M, Righi E, Lindstrom V, Leblanc PR, Poznansky MC. HIV-1 envelope protein gp120 is present at high concentrations in secondary lymphoid organs of individuals with chronic HIV-1 infection. J Infect Dis. 2009;200:1050–3. https://doi.org/10.1086/605695.
24. Mintun MA, Raichle ME, Kilbourn MR, Wooten GF, Welch MJ. A quantitative model for the in vivo assessment of drug binding sites with positron emission tomography. Ann Neurol. 1984;15:217–27. https://doi.org/10.1002/ana.410150302.
25. Chapman AP. PEGylated antibodies and antibody fragments for improved therapy: a review. Adv Drug Deliv Rev. 2002;54:531–45. https://doi.org/10.1016/s0169-409x(02)00026-1.
26. O'Donoghue JA, Danila DC, Pandit-Taskar N, Beylergil V, Cheal SM, Fleming SE, et al. Pharmacokinetics and Biodistribution of a [(89)zr]Zr-DFO-MSTP2109A Anti-STEAP1 antibody in metastatic castration-resistant prostate Cancer patients. Mol Pharm. 2019;16:3083–90. https://doi.org/10.1021/acs.molpharmaceut.9b00326.
27. Mulligan T, Carrasquillo JA, Chung Y, Milenic DE, Schlom J, Feuerstein I, et al. Phase I study of intravenous Lu-labeled CC49 murine monoclonal antibody in patients with advanced adenocarcinoma. Clin Cancer Res. 1995;1:1447–54.
28. Horiike M, Iwami S, Kodama M, Sato A, Watanabe Y, Yasui M, et al. Lymph nodes harbor viral reservoirs that cause rebound of plasma viremia in SIV-infected macaques upon cessation of combined antiretroviral therapy. Virology. 2012;423:107–18. https://doi.org/10.1016/j.virol.2011.11.024.
29. Keenan AM, Weinstein JN, Carrasquillo JA, Bunn PA Jr., Reynolds JC, Foon KA, et al. Immunolymphoscintigraphy and the dose dependence of 111In-labeled T101 monoclonal antibody in patients with cutaneous T-cell lymphoma. Cancer Res. 1987;47:6093–9.
30. Omidvari N, Jones T, Price PM, Ferre AL, Lu J, Abdelhafez YG, et al. First-in-human immunoPET imaging of COVID-19 convalescent patients using dynamic total-body PET and a CD8-targeted minibody. Sci Adv. 2023;9:eadh7968. https://doi.org/10.1126/sciadv.adh7968.
31. Bray M, Di Mascio M, de Kok-Mercado F, Mollura DJ, Jagoda E. Radiolabeled antiviral drugs and antibodies as virus-specific imaging probes. Antiviral Res. 2010;88:129–42. https://doi.org/10.1016/j.antiviral.2010.08.005.
32. Bhaumik S, Walls Z, Puttaraju M, Mitchell LG, Gambhir SS. Molecular imaging of gene expression in living subjects by spliceosome-mediated RNA trans-splicing. Proc Natl Acad Sci U S A. 2004;101:8693–8. https://doi.org/10.1073/pnas.0402772101.
33. Madden PJ, Thomas Y, Blair RV, Samer S, Doyle M, Midkiff CC et al. An immunoPET probe to SARS-CoV-2 reveals early infection of the male genital tract in rhesus macaques. bioRxiv. 2022:2022.02.25.481974. https://doi.org/10.1101/2022.02.25.481974

Publisher's note Springer Nature remains neutral with regard to jurisdictional claims in published maps and institutional affiliations.